Universality classes of thermalization for mesoscopic Floquet systems

Alan Morningstar [1,2] David A. Huse [1] and Vedika Khemani [2]
[1]*Department of Physics, Princeton University, Princeton, New Jersey 08544, USA*
[2]*Department of Physics, Stanford University, Stanford, California 94305, USA*

(Received 9 December 2022; accepted 23 October 2023; published 9 November 2023)

We identify several distinct phases of thermalization that describe regimes of behavior in isolated, periodically driven (Floquet), mesoscopic quantum chaotic systems. In doing so, we also identify a Floquet thermal ensemble, the "ladder ensemble," that is qualitatively distinct from the "featureless infinite-temperature" state that has long been assumed to be the appropriate maximum-entropy equilibrium ensemble for driven systems. The phases we find can be coarsely classified by (i) whether or not the system irreversibly exchanges energy of order ω with the drive, i.e., *Floquet thermalizes*, and (ii) the *Floquet thermal ensemble* describing the final equilibrium in systems that do Floquet thermalize. These phases are representative of regimes of behavior in mesoscopic systems, but they are sharply defined in a particular large-system limit where the drive frequency ω scales up with system size N as the $N \to \infty$ limit is taken: we examine frequency scalings ranging from a weakly N-dependent $\omega(N) \sim \log N$, to stronger scalings ranging from $\omega(N) \sim \sqrt{N}$ to $\omega(N) \sim N$. We show that the transition where Floquet thermalization breaks down happens at an extensive drive frequency and, beyond that, systems that do not Floquet thermalize are distinguished based on the presence or absence of rare resonances across Floquet zones. We produce a thermalization phase diagram that is relevant for numerical studies of Floquet systems and experimental studies on small-scale quantum simulators, both of which lack a clean separation of scales between N and ω. A striking prediction of our work is that, under the assumption of perfect isolation, certain realistic quench protocols from simple pure initial states can show Floquet thermalization to a type of Schrodinger-cat state that is a global superposition of states at distinct *temperatures*. Our work extends and organizes the theory of Floquet thermalization, heating, and equilibrium into the setting of mesoscopic quantum systems.

DOI: 10.1103/PhysRevB.108.174303

I. INTRODUCTION

Breakthrough experimental developments in building isolated quantum systems have led to significant recent progress in quantum statistical mechanics. This has fueled advances in our understanding of fundamental questions surrounding the process of *thermalization* and its various exceptions in isolated many-body systems [1–7].

In the common case of a system governed by a time-independent Hamiltonian, the system thermalizes if, at late times, probability distributions of local observables are indistinguishable from those in a relevant thermal ensemble. The appropriate thermal ensemble is determined by the principle of entropy maximization, constrained by the conservation laws of the system. The eigenstate thermalization hypothesis (ETH) [1,8–13] posits conditions for thermalization on individual eigenstates of the dynamics, and empirically these conditions hold in examples of thermalizing systems [14–19].

Upon the addition of a periodic drive of frequency ω, i.e., making the system "Floquet," the Hamiltonian and eigenstates of the stroboscopic dynamics gain a periodic time dependence. The drive breaks the conservation of energy and the appropriate long-time maximum-entropy equilibrium is assumed to be a *featureless* "infinite-temperature" state [20,21]. Exceptions to this "heat death" are possible [22,23], notably in many-body localized (MBL) or integrable Floquet systems [24–27], in which case the system may thermalize to a generalized periodic Gibbs ensemble [28,29] and/or realize novel ordered phases such as the discrete time-crystal [30–34] or the anomalous Floquet insulator [35,36]. Heating can also be suppressed for a time exponential in the drive frequency, a transient phenomenon called Floquet prethermalization [37–50]. All of these results on Floquet thermalization and its exceptions were obtained in works aimed at the limit where the drive frequency ω is finite and the number of degrees of freedom in the system N is infinite.

However, as we show in this paper, this limit provides an incomplete description of thermalization in chaotic Floquet systems. In particular, in *mesoscopic* systems where N is finite, there are other regimes of thermalization captured by thermal ensembles that are *qualitatively distinct* from a featureless infinite-temperature state. These regimes, and the crossovers between them, occur at drive frequencies that depend on the system size N, so to study them we allow for a drive frequency $\omega \propto \Omega(N)$ that is scaled up with N. We examine frequency scalings ranging from a weakly N-dependent $\Omega(N) = \log N$, to stronger scalings ranging from $\Omega(N) = \sqrt{N}$ to $\Omega(N) = N$. The distinctions between the different regimes we obtain can be made sharp in a particular large-N limit [51–55], discussed later, where $N \to \infty$ is taken with $\omega/\Omega(N)$ held constant, i.e., a large-ω limit is taken at the same time.[1] This limit may appear nonstandard when

[1]The width of the crossovers [in the control parameter $\omega/\Omega(N)$] scales as $\Omega(N)^{-1}$ and sharpens up as the limit is taken.

compared to conventional thermodynamic limits studied in many-body physics, but is standard in studies of mesoscopic systems where interaction strengths and/or other parameters are often taken to scale with N [51].

One motivation for studying the different possible regimes of thermalization in mesoscopic Floquet systems is that many settings, for instance, experiments on near-term quantum simulators, allow controlled access to "intermediate-scale" [56] many-body quantum systems where there is not a clean separation of scales between N and ω (measured in units of a microscopic energy scale). This is also true for numerical studies of Floquet phenomena, which are limited to small system sizes [57]. There is currently a major gap in the literature in theoretically and systematically addressing thermalization, Floquet heating, and equilibrium in this setting, which we hope to bridge with this work.

A. Summary of results

We identify a number of distinct regimes of thermalization, and crossovers between them, that can occur in mesoscopic Floquet systems. In this work, we are only considering isolated chaotic many-body systems subject to periodic driving, focusing on the delocalization of energy across Floquet zones; in particular, all the crossovers we consider are between chaotic regimes with different degrees of energy conservation, so the physics of many-body localization or integrability will play no role in our discussion. Reference [58] instead considers the fate of finite-size driven integrable systems, with an N-dependent driving amplitude. The different regimes of thermalization we find are summarized below and in Fig. 1(a), and explained in detail later:

(i) At the smallest frequencies, the system irreversibly exchanges energy with the drive and Floquet thermalizes to a conventional *featureless infinite-temperature* state, i.e., the relevant Floquet thermal ensemble is a uniform distribution over all states [Fig. 1(b)].

(ii) At larger frequencies, beyond $\omega = \omega_{\text{ladder}}(N) \sim \log N$ [or, in some physically relevant cases discussed later, $\omega_{\text{ladder}}(N) \sim \sqrt{N}$], the system instead Floquet thermalizes to a *ladder ensemble*. In this regime, energy conservation is not completely destroyed, but downgraded to an approximate conservation of energy modulo ω. Thus, energy becomes delocalized across a "ladder" of narrow energy windows that are spaced by ω. This is the relevant maximum-entropy Floquet thermal ensemble under the constraint of conservation of energy modulo ω [Fig. 1(c)]. While in some cases this ensemble can have the same average energy as the infinite-temperature ensemble, the distribution of energy is distinct.

(iii) At yet larger frequencies beyond $\omega = \omega_{\text{partial}}(N) \sim N$, the system only partially thermalizes across the rungs of the ladder. We call this the regime of *partial Floquet thermalization*. In this regime, a version of Floquet heating may still occur for many initial states.

(iv) Finally, at the largest frequencies, beyond $\omega = \omega_{\text{loc}}(N) \sim N$, the system does not exchange energy of order ω or more with the drive, i.e., it does not Floquet thermalize and instead becomes *energy localized*. In this regime, there exists an extensive energy, defined by a quasilocal effective Hamiltonian, that is approximately conserved for all times.

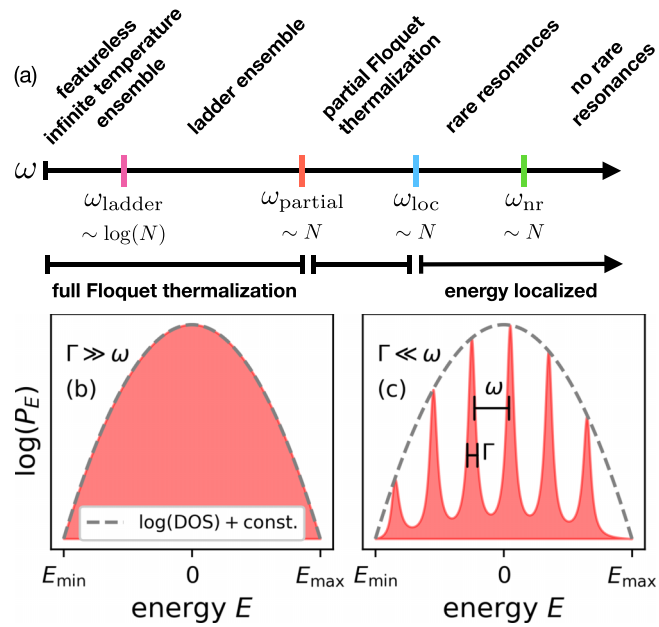

FIG. 1. Distinct regimes of thermalization in mesoscopic Floquet systems. (a) A sketch of the different regimes of thermalization, listed in Sec. I A. The various frequencies marked along the axis depend on the system size N as shown, and also on (quasi) energy, so the line shown is a cut through the full 2D phase diagram of Fig. 2. (b), (c) A depiction of the (b) "featureless infinite-temperature" and (c) "ladder" ensembles. These are probability distributions over a suitable definition of energy (for example, an effective Hamiltonian) that can be relevant descriptions of the final equilibrium of a Floquet system. In the featureless ensemble (b), the distribution over energy follows the density of states. In contrast, for the ladder ensemble, the distribution of energy is peaked (with peak widths Γ) around energies with the same E mod ω. The weights of the peaks follow the density of states (DOS) at those energies, $P_E \propto \text{DOS}(E)$. The featureless ensemble corresponds to a loss of energy conservation under the Floquet dynamics, while the ladder ensemble corresponds to maintaining an approximate conservation of E mod ω.

While the extensive many-body bandwidth furnishes an upper bound for $\omega_{\text{loc}}(N)$, we find that energy localization sets in at a smaller scale, and distinct nontrivial energy-localized regimes exist that can be distinguished by the presence or absence of isolated Floquet many-body resonances in rare states.

A few points are of note. First, complete Floquet thermalization occurs for frequencies less than $\omega_{\text{partial}}(N) \sim N$, in the sense that the system effectively exchanges energy with the drive. In most of this regime, i.e., between the two scales $\omega_{\text{ladder}}(N) \sim \log(N)$ and $\omega_{\text{partial}}(N) \sim N$, the ladder ensemble is the relevant description of the final thermal equilibrium. In contrast, the regime in which the system thermalizes to a featureless infinite-temperature state is parametrically smaller, extending only up to $\omega_{\text{ladder}}(N) \sim \log(N)$. Second, while we have only focused on the frequency dependence of the different regimes in the discussion above [and in Fig. 1(a)], there is also a strong dependence on (quasi)energy which we explore below. In Fig. 2, we map out the full two-parameter phase diagram of the different types of thermalization mentioned above, and one important message of our work is that sometimes the thermalization of Floquet systems needs to be state

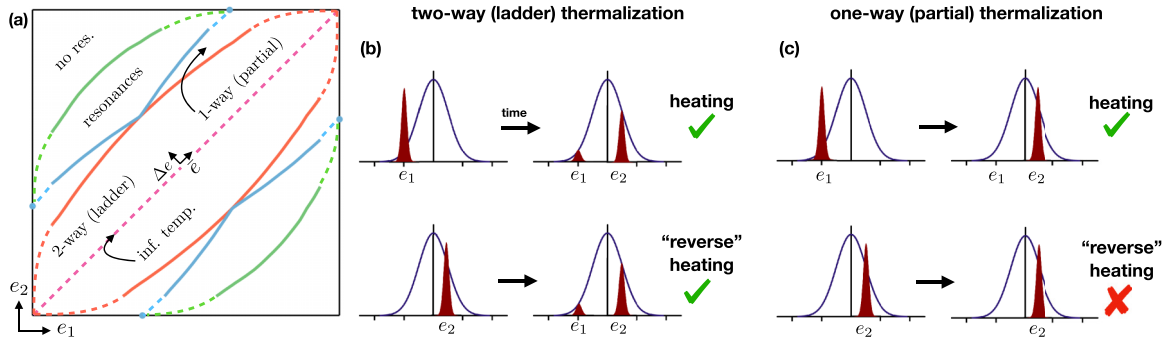

FIG. 2. Phases of thermalization in Floquet systems. (a) The phase diagram in the two-zone approximation. The purpose of this diagram is to show the qualitative organization of the phases, but we have used numerical data from simulations of small systems to draw the curves for concreteness. The solid lines are obtained using only $N \in \{12, 14\}$ data, and the dashed curves are sketched extrapolations. For example, the middle of the red curve corresponds to the point at which the $N = 12$ and 14 curves of Fig. 4 intersect. See Sec. III C for a full description. The outer black square marks the edges of the spectrum of H_0. A point on the diagram specifies two energy densities, e_1 and e_2, which can also be labeled by $\bar{e}$ and Δe (i.e., the frequency $\omega = N\Delta e$ is implied by the point, and is constant along lines of constant Δe). The phase which that point belongs to indicates the extent to which the Floquet dynamics mixes those two energy densities. The pink dashed line denotes $\Delta e = 0$, which contains the commonly considered case of finite ω and $N \to \infty$. The distinct behaviors are as described in Fig. 1(a) and in the main text. The terms "resonances" and "no res." indicate energy-localized phases with and without rare Floquet resonances. (b), (c) Depictions of two-way and one-way thermalization. In two-way thermalization, initial states at either energy density thermalize to have the correct equilibrium populations at those energies. In one-way thermalization, states at a high density of states do not decay into a window of energy at a much lower density of states, so there is heating but not the "reverse heating" needed to produce full Floquet thermalization.

or energy resolved instead of uniformly averaging over all Floquet eigenstates or initial states.

Finally, a notable consequence of our results is that under a suitable quench protocol, isolated systems in pure states can thermalize to *Schrodinger cat states of temperature*, i.e., superpositions of states at globally different energy *densities* [Fig. 1(c)]. Although the coherences of such states are notoriously fragile, the ladderlike distribution of energy is a stable signature of this form of Floquet thermalization.

The rest of this paper is organized as follows: In Sec. II we set up our theoretical understanding of the different regimes of thermalization that occur in mesoscopic Floquet many-body quantum systems. We support our theoretical reasoning with numerical evidence using a concrete model in Sec. III. In Sec. IV we explore some of the prospects for studying the physics discussed in this work experimentally, and show that indeed experimental studies seem to be accessible on some near-term platforms for quantum simulation. Finally, we summarize and discuss our findings in Sec. V.

II. THEORY

A. Setup and review of Floquet heating

For the purpose of discussion, we consider N qubits evolving under a time-periodic Hamiltonian $H(t) = H_0 + g_\omega(t)V_0$, where g_ω is an $O(1)$-valued periodic function of time that time averages to zero, with period $T = \frac{2\pi}{\omega}$. The most basic case to consider is a monochromatic $g_\omega(t)$, with weight only on the frequency ω, e.g., $\cos(\omega t)$, but higher harmonics can also be present, e.g., $\text{sign}[\cos(\omega t)]$. H_0 is a quantum chaotic Hamiltonian that is a sum of one- and two-body terms, and V_0 couples the system to the drive, also consisting of a sum of one- and two-body terms. A characteristic microscopic energy scale of H is set to one here. We are generally interested in behavior at $\omega \gg 1$, although in practice $\omega \gtrsim \omega_0$ can be a more accurate condition, where ω_0 is $O(1)$ and depends on the specific system. Both H_0 and V_0 are traceless, so the energy corresponding to infinite temperature is zero. $\frac{1}{N2^N}\text{tr}(H_0^2)$, $\frac{1}{N2^N}\text{tr}(V_0^2)$, and $\frac{1}{N2^N}\text{tr}([H_0, V_0]^2)$ are all of order one, so the only small parameters present are $1/\omega$ and $1/N$. The stroboscopic dynamics are governed by the Floquet unitary $U_F = \mathcal{T}\exp(-i\int_0^T H(t)dt)$ that time evolves the system by one period. The Floquet unitary defines the Floquet Hamiltonian H_F via $U_F \equiv \mathrm{e}^{-iH_F T}$. The quasienergies θ are defined such that the eigenvalues of U_F are $\mathrm{e}^{-i\theta T}$, so θ is only defined modulo ω and is strictly conserved by the dynamics, and this may be the only such strict conservation law. The specific model we use for later numerical demonstrations is given in Sec. III, but our results are more general.

The process of Floquet heating entails a system resonantly exchanging energy with the drive in quanta of size $\sim\omega$. In this work, we will ideally consider frequencies ω that are large compared to the microscopic energy scale of H, which is set to 1 here [the regime when ω is comparable to the local energy scales leads to rapid heating, but the $\omega \sim O(1)$ boundary between these two regimes is system dependent]. In this high-frequency regime, absorbing a quanta $\sim\omega$ of energy requires a high-order process involving $O(\omega)$ local energy moves, which occurs at a rate that is exponentially suppressed in ω. Because these processes can happen anywhere in the system, the system as a whole exchanges "photons" with the drive at a rate [37–41]

$$\Gamma \sim N\mathrm{e}^{-\omega/\omega_0}, \tag{1}$$

with some microscopic (order one) ω_0 that may, in general, depend on the energy density.[2] This is the behavior in the

[2]In one dimension there is a logarithmic correction such that the heating rate is bounded by $\Gamma \sim N\mathrm{e}^{-(\omega\log\omega)/\omega_0}$ [59–61]. We focus

drive frequency range $\omega_0 \lessapprox \omega \ll N\omega_0$, and, in this regime, there is an effective ("prethermal") quasilocal Hamiltonian H_{eff} that captures the dynamics of the system on timescales shorter than $t \sim \Gamma^{-1}$. H_{eff} can be obtained perturbatively, and represents the most optimal quasilocal truncation of a high-frequency Magnus expansion for H_F [39]. The leading term in the expansion is the time-averaged Hamiltonian H_0 (see Appendix A).

The timescale Γ^{-1} sets the crossover time between the prethermal regime with dynamics governed by H_{eff} (which has an extensive conserved energy), and the regime of *Floquet thermalization*, where the system thermalizes *across* different Floquet zones due to a resonant drive-mediated coupling between states separated in energy by ω and therefore becomes delocalized in energy [23]. The slow thermalization across Floquet zones is reflected in the nonperturbative, nonlocal character of H_F. The difference between $U_F = e^{-iH_F T}$ and $e^{-iH_{\text{eff}} T}$ is the thermalization process across Floquet zones visible on times $t > \Gamma^{-1}$.

B. Floquet thermal ensembles and nonstandard large-N limits

We now discuss the featureless infinite-temperature and ladder ensembles for Floquet thermalization, the crossover between these, and how this crossover sharpens in a particular large-N limit.

For a system that absorbs or emits energy slowly enough, an eigenstate of U_F with eigenvalue $e^{-i\theta T}$ will be supported on eigenstates of H_{eff} near a "ladder" of energies that differ in steps of ω, i.e., with energies

$$E_{\text{eff}} = \theta \pm n\omega \tag{2}$$

with $n \in \mathbb{Z}$. However, due to the nonzero heating rate, each of the "rungs" of the energy ladder will have an energy uncertainty $\sim \Gamma \sim N e^{-\omega/\omega_0}$ [see Fig. 1(c) for a depiction]. In the commonly prioritized limit of finite ω and $N \to \infty$, the rate Γ grows with N and eventually becomes larger than ω (when $N \sim \omega e^{\omega/\omega_0}$). For N well in excess of this, the ladder is not resolvable as the width of the rungs exceeds the spacings between rungs, and the energy conservation (even modulo ω) is fully lost. The resulting equilibrium is then "infinite temperature" in a strict sense because the relevant Floquet thermal ensemble is a uniform distribution over all energy eigenstates, as shown in Fig. 1(b).

The strict infinite-temperature property of Floquet thermalized states (and eigenstates of U_F) can break down to various degrees when $\Gamma \ll \omega$. This can occur in systems with finite N and ω, or in large-N systems where we allow ω to scale up with N in such a way that some behavior characteristic of finite-size systems is retained in the limit. For example, consider $\omega_{\text{ladder}}(N) = \omega_0 \log N$: If ω is scaled up with N faster, so that $\omega \gg \omega_{\text{ladder}}(N)$, then $\Gamma \ll \omega$ at large enough N. In this regime, the distributions of energy in the eigenstates of U_F have significant weight only near a well-resolved ladder of energies with spacing ω, as shown in Fig. 1(c). In other words, the energy defined by H_{eff} is conserved modulo ω to a precision of $\sim \Gamma$.

This "energy ladder" is a maximum-entropy Floquet thermal ensemble that is distinct from "infinite temperature" and notably it sets in already at a frequency scale $\omega_{\text{ladder}} = \omega_0 \log N$ that is only weakly dependent on N. If we consider the rescaled frequency $\nu = \frac{\omega}{\omega_{\text{ladder}}(N)} = \frac{\omega}{\omega_0 \log N}$, then the crossover from the featureless infinite-temperature ensemble to the ladder ensemble happens near $\nu = 1$. This crossover in the rescaled variable ν becomes sharp in the large-N limit as can be seen from the behavior of $\frac{\Gamma}{\omega} = \frac{N e^{-\omega/\omega_0}}{\omega} = \frac{N^{1-\nu}}{\nu \omega_0 \log(N)}$ near $\nu = 1$: it diverges with N if $\nu < 1$ and approaches zero if $\nu > 1$.

The ladder ensemble sets in at $\omega \sim \log(N)$ and extends to parametrically larger frequency scalings $\omega = \omega_{\text{partial}}(N) \sim N$. First consider $\omega \sim N^\alpha$, with $0 < \alpha < 1$. As long as $\alpha < 1$, consecutive rungs on the ladder have different energies but the same energy *density* as $N \to \infty$, i.e., the spacing in energy density between the rungs tends to zero. Each Floquet quasienergy θ corresponds to populating a ladder of energies $E_{\text{eff}} \bmod \omega = \theta$ that spans across all energy densities. In particular, the ladder contains a subset of rungs that have the same energy (and entropy) *density* as infinite temperature in the $N \to \infty$ limit, $E^{\infty}_{\text{eff}}/N = \frac{1}{N 2^N} \text{Tr}[H_{\text{eff}}] = 0$. Thus, the final equilibrium is one where the *average* energy density corresponds to infinite temperature, but the *distribution* of energy is markedly distinct from the uniform distribution and instead concentrated near a ladder of well-spaced energies.

Finally, we have the case of $\omega \propto N$ ($\alpha = 1$). In this case, the frequency ω is extensive and corresponds to transitions between different *energy densities* e; thus we denote $\Delta e \equiv \frac{\omega}{N}$ in the rest of this paper. Since ω is extensive in this case, it is not generally true that the system thermalizes to the same average energy density as infinite temperature in the $N \to \infty$ limit, even when it does equilibrate across Floquet zones (Floquet thermalizes). This is because the final energy distribution resides on a ladder of different energy densities, and the infinite temperature energy density ($e = 0$) is not generally one of them (see Fig. 5 for a demonstration).

This brings us to an important point: Floquet thermalization (also referred to as Floquet heating) refers to reaching the appropriate equilibrium ensemble with energies distributed either according to the uniform infinite-temperature ensemble or the appropriate ladder ensemble. The ladder ensemble is always a distinct ensemble from infinite temperature, and need not even have the same average energy density as infinite temperature. *Thus, Floquet thermalization does not imply that the system thermalizes to infinite temperature, even on average.*

Some comments are in order before concluding this section. When defining the ladder ensemble, we considered energies defined according to H_{eff}, the most optimal quasilocal truncation of H_F. In this case, the energy defined by H_{eff} is conserved modulo ω to a precision of $\sim \Gamma$ set by the heating rate. However, if H_{eff} is not chosen optimally, for instance, if energy is defined with respect to the leading term H_0, then the precision is lower and the width of the rungs is accordingly broader, as discussed in Appendix A. Likewise, if we consider thermalization of generic initial states (instead of eigenstates

on the general case in higher dimensions for our discussion and numerical studies below, but the results are qualitatively the same in one dimension.

of U_F), then the energy uncertainty of the initial state also contributes to the broadening of the rungs. A typical product initial state has energy uncertainty $\propto \sqrt{N}$, and hence requires $\omega \sim N^\alpha$ with $\alpha > \frac{1}{2}$ to resolve the rungs of the ladder for large enough N. In this case, the crossover from the featureless infinite-temperature ensemble to the ladder ensemble happens at $\omega_{\text{ladder}}(N) \sim \sqrt{N}$ and it does not sharpen up in the large-N limit.

In sum, in this section we have discussed different Floquet thermal ensembles that are relevant for the different ways in which a system can Floquet thermalize. This has been in the context of mesoscopic systems, but also using the notion of nonstandard large-N limits, with N-dependent frequencies, that help us sharply distinguish the different regimes. As also mentioned, beyond a certain scale $\omega_{\text{loc}} \propto N$, Floquet thermalization does not occur and the effect of the drive is perturbative for almost all eigenstates. In those cases, energy is localized to the microcanonical window of states near the initial energy, which is conserved.

In the next section, and in much of the rest of the paper, our goal is to map out a phase diagram delineating various thermal and nonthermal Floquet regimes. In order to do this, we discuss the structure present *at* the scaling $\omega \propto N$, where both Floquet thermalization and various partially thermalizing or non-Floquet-thermal phases exist in the large-N and large-ω limits. Note that at this scale, we are no longer probing the crossover between the infinite-temperature and ladder ensembles (which happens at parametrically smaller frequencies); instead, our goal is to study different degrees of thermalization to the appropriate ladder ensemble.

C. Thermalization phase diagram

Our goal is to map out the various types of thermalization that can occur in mesoscopic Floquet systems and, relatedly, in Floquet systems in nonstandard large-N limits. In the former, these are regimes of behavior with smooth crossovers between them, while in the latter they are idealized sharp phases representative of the finite-$N$and -ω regimes. To do this we fix $\omega \propto N$ and consider the matrix elements of the drive operator V_0 between eigenstates of H_0 separated in energy density by Δe, and the relevant density of states of H_0, in order to argue for or against interzone thermalization and Floquet resonances. Note that the rungs of the ladder represent different Floquet zones, so thermalization to the ladder ensemble corresponds to interzone thermalization. We use the leading order H_0 as our definition of energy because $H_{\text{eff}} \to H_0$ as $N, \omega \to \infty$, and because it is the simplest option, e.g., using H_0 results in a notion of energy that is not ω dependent, as H_{eff} is (also see the discussion in Appendix A). We also corroborate our findings numerically with the full dynamics generated by U_F for our model system in Sec. III.

We refer to the inverse energy-level spacing of H_0 as the density of states (DOS), so that it is the number density, in energy (not in energy and volume), of many-body energy levels. At large N, the DOS of H_0 is of the form

$$D(e) = \exp[Ns(e)], \tag{3}$$

up to subexponential factors, where $s(e)$ is the entropy density at energy density e.

A similar form is motivated for the matrix elements of V_0, which are suppressed exponentially in ω [19,62,63], in accordance with the exponentially slow heating rate. As we are considering $\omega \propto N$ now, the matrix elements are exponentially small in N for a fixed Δe. Therefore, we assume that the leading behavior of the size of the matrix elements is

$$V(e_1, e_2) = \exp[-Nf(\Delta e, \bar{e})], \tag{4}$$

where e_1 and e_2 are the energy densities of the two eigenstates of H_0, and f is a function of the difference and mean

$$\Delta e = \frac{\omega}{N} = |e_2 - e_1| \text{ and } \bar{e} = \frac{e_1 + e_2}{2}. \tag{5}$$

Note that the form of Eq. (4) matches to the ETH [1] and to the heating behavior discussed above, with $f(\Delta e, \bar{e}) \cong \frac{1}{2}[s(\bar{e}) + \frac{\Delta e}{\omega_0}]$ for small Δe. However, here we are dealing with matrix elements between extensively different energies, so we allow a more general form for f.

We have now completed the essential setup for understanding the main features of the thermalization phase diagram, which we explain here and support with numerical evidence in Sec. III. The presence or absence of thermalization and/or resonances between Floquet zones should be governed by comparing the relevant energy-level spacing with the relevant matrix elements or rates for those processes. When the frequency is extensive, this comparison is nontrivial because the exponents in Eqs. (3) and (4) are both $\propto N$.[3]

Since the frequency and many-body bandwidth of H_0 are both extensive in N, the number of rungs in the relevant ladder ensemble is finite. To simplify the analysis, we truncate the ladder to two rungs and work in a *two-zone approximation*, where we consider Floquet thermalization and resonances involving two narrow windows of energy density near e_1 and e_2 (this implies the frequency via $\omega = N|e_1 - e_2|$, and the quasienergy via $\theta = Ne_1 \bmod \omega$), and we discuss the minor modifications that come with considering the rest of the Floquet zones in the energy-density ladder in Appendix C. We find four distinct phases, ordered from the most thermalizing to the least: "two-way (full) thermalization," "one-way (partial) thermalization," and two energy-localized phases with "isolated resonances," and with "no resonances." The phase with two-way Floquet thermalization contains a sliver of vanishing relative size that is thermalization to the infinite-temperature ensemble or to a ladder ensemble with zero average energy density. The phase diagram is shown in Fig. 2; we will explain the ideas behind each phase below, and support the diagram with numerical evidence later on.

[3]In one dimension there is a correction such that $\omega \propto N/\log N$ (a slightly subextensive frequency) is instead the scaling needed to have $(1/D)$ and V scale similarly [59–61]. We proceed with the $\omega \propto N$ scaling presented above, which appears to be correct for systems in more than one dimension, and is consistent with the numerics for an all-to-all quantum dot model that we study below. The finite-size regimes in our phase diagram are all still present for the modified scaling in one dimension, although the precise scaling of ω needed to remain in any one of the phases as one takes the large-N limit is slightly altered by the $1/(\log N)$ factor.

1. Two-way (full) thermalization

In the phase with two-way Floquet thermalization, states at e_1 and e_2 get fully mixed by the presence of the drive in the sense that in the $N \to \infty$ limit, any initial state at either energy density will thermalize to occupy states at both energy densities with weight proportional to $D(e_1)$ and $D(e_2)$, respectively. Another way of saying this is that the Floquet eigenstates of U_F will all have weight on both rungs of the corresponding energy ladder, with weights proportional to the DOS.

This phase occurs when the rate for transitioning from one energy to the other is larger than the level spacing at the initial energy, a symmetric condition given by $\lim_{N\to\infty} V(e_1, e_2)^2 D(e_1) D(e_2) = \infty$. Using Eqs. (3) and (4) this translates to

$$2f(\Delta e, \bar{e}) < s(e_1) + s(e_2). \tag{6}$$

Intuitively, this says that each energy has a high enough density of states that states at the other energy "see" them as an effective continuum and transition to them at a Fermi golden rule (FGR) rate [62–66]. If we label e_2 as the energy closer to zero with higher DOS, so that $D(e_2) \geqslant D(e_1)$, then FGR is valid for transitions from e_1 to e_2, so that a system initialized at e_1 thermalizes to acquire weight at both e_1 and e_2 in proportion to the DOS at the two energies. We call this process "heating" since the e_2 is at a higher (absolute value of) temperature than e_1. Due to the heating process, the resultant broadening of the levels at the lower DOS is larger than the level spacing there, thus both DOS act as a continuum. As a result, a state initialized at e_2 would also thermalize to acquire a small weight on e_1 that is proportional to $D(e_1)$, a process we called "reverse heating" [see Fig. 2(b)]. In general, since the DOS is exponentially larger (in N) for e_2, the system thermalizes on average to e_2, the energy with the higher entropy density, when N is large.

A special case occurs when $D(e_1) = D(e_2)$. This occurs in models with $D(e) = D(-e)$ when both energies are situated symmetrically about zero, so that $e_2 = -e_1 = \frac{\omega}{2N}$. This corresponds to Floquet eigenstates at eigenvalue $\mathrm{e}^{-i\theta T} = \mathrm{e}^{i\frac{\omega}{2}\frac{2\pi}{\omega}} = -1$, i.e., with quasienergy $\theta = \pi/T$. In this case, the final thermal equilibrium is an equal-weight superposition of two different energy densities, one corresponding to positive temperature and the other to negative temperature. Because the final equilibrium is a superposition of states in two well-separated narrow energy windows, and those states look locally like they are described by the Boltzmann distribution, this final local Floquet equilibrium is approximately described by

$$\rho = \frac{1}{2Z}\left(e^{-\beta H_0} + e^{\beta H_0}\right) = \frac{1}{Z}\cosh(\beta H_0), \tag{7}$$

where the inverse temperature β is set by e_1. This is a different type of Floquet ETH ensemble distinct from infinite temperature: even though the average energy corresponds to that of infinite temperature, the distribution is bimodal with weight at positive and negative temperature states, and almost no weight at zero energy [see Fig. 5(a)].

A consequence of this is that if we start with a simple initial *pure* state at energy E_1 and drive it with frequency $2|E_1|$, the state will thermalize to spontaneously become a type of pure *Schrodinger-cat state of temperature*, i.e., a global superposition of thermal pure states at two different temperatures! While the coherences of such states are extremely sensitive to imperfect isolation, the ladderlike distribution of energy is a much more robust signal of this type of Floquet thermalization. We explore the prospects of realizing these equilibrium distributions experimentally in Sec. IV.

2. One-way (partial) thermalization

The phase with one-way, or partial, Floquet thermalization is subtly different in that the higher entropy density appears as a continuum to the lower, but the converse is not true. The condition for this phase is the validity of Fermi's golden rule (FGR) in one direction but not the other, which translates to

$$s(e_1) + s(e_2) < 2f(\Delta e, \bar{e}) < 2s(e_2), \tag{8}$$

if we label the higher DOS as e_2. This is equivalent to $V(e_1, e_2)^2 D(e_1) D(e_2)$ vanishing with N but $V(e_1, e_2)^2 D(e_2)^2$ diverging. Under this condition, a system initialized at e_1 would heat to thermalize to e_2, as in the two-way phase, but a state initialized at e_2 would generally not thermalize to acquire a small weight on e_1 that is proportional to $D(e_1)$ [Fig. 2(c)]. Such a subtle entropically suppressed "reverse heating" could be unimportant if N is large, due to $D(e_1) \ll D(e_2)$. In that case, the union of the phases with one-way and two-way Floquet thermalization is the more physically important concept.

3. Energy localized

We now move on to the two remaining phases where Floquet thermalization fails, so they are energy localized. This sets in when

$$s(e_1),\ s(e_2) < f(\Delta e, \bar{e}). \tag{9}$$

This condition means that typical states no longer couple to other Floquet zones under the dynamics. Notably, our arguments show transparently why the boundary of the energy-localized regime occurs at an extensive frequency because both $V(e_1, e_2)$ and $D(e)$ scale exponentially with N. In particular, this rules out other seemingly plausible scalings such as $\omega_{\mathrm{loc}} \propto \sqrt{N}$ which could be argued for, for instance, by comparing the frequency to the standard deviation in energy of the DOS [21].

The energy-localized phase is further divided into two phases distinguished by the presence or absence of rare Floquet many-body resonances [67], by which we mean rare Floquet eigenstates U_F that are superpositions of eigenstates of H_0 in different Floquet zones, while most eigenstates are energy localized. Unlike the matrix elements responsible for many-body resonances in many-body localized systems, which can have very broad distributions [68–71], the distribution of the matrix elements of V_0 between energy eigenstates of H_0 at e_1 and e_2 should be Gaussian and thus well characterized by a single value $V(e_1, e_2)$ because the energy eigenstates of H_0 are thermal. Thus, the expectation of any rare Floquet many-body resonances is heralded by comparing the size of these matrix elements to the smallest energy gap $E_2 - E_1 - \omega$, where $E_{1,2}$ are within the energy windows we have been discussing. The minimum gap scales as $[D(e_1)D(e_2)]^{-1}$, so such

rare resonances are expected to be present in typical samples in the energy-localized phase with isolated resonances, the condition for which is

$$s(e_1),\ s(e_2) < f(\Delta e, \bar{e}) < s(e_1) + s(e_2). \tag{10}$$

When $f(\Delta e, \bar{e})$ is even larger than $s(e_1) + s(e_2)$, the system is in the "no resonances" phase, which also contains the trivial regime of e and ω such that both $(e + \Delta e)$ and $(e - \Delta e)$ are outside of the many-body bandwidth of the system, and H_{eff} is good for describing the dynamics of all states for all times (there is no nonperturbative effect of the periodic drive).

4. Crossovers

The relevant quantities governing the crossovers between the phases discussed in this section all have the form

$$e^{N[as(e_1)+bs(e_2)-cf(\Delta e,\bar{e})]} \tag{11}$$

for integers a, b, and c (up to subexponential corrections). This is because all the conditions derived in Eqs. (6)–(10) were obtained by comparing powers of matrix elements and DOS, which have the exponential forms shown in Eqs. (4) and (3).

This implies that as we tune through the crossovers by varying, e.g., $\Delta e = \omega/N$, their widths sharpen up as $\propto N^{-1}$, which superficially looks like a transition with critical exponent $\nu = 1$. However, to the best of our knowledge this scaling does not correspond to any diverging length scale and associated critical exponent ν, and thus these sharp crossovers are not like continuous phase transitions in that sense.

In this and the previous sections, we have explained our theoretical understanding of the idealized phases that represent different regimes of Floquet thermalization and many-body resonances that occur in isolated mesoscopic periodically driven systems. In the next section, we corroborate these ideas with numerical evidence to obtain the phase boundaries for the different phases plotted in the phase diagram in Fig. 2(a).

III. NUMERICAL EVIDENCE

As a model system we take N-qubit degrees of freedom evolving under the time-periodic Hamiltonian

$$H(t) = H_0 + \text{sgn}[\cos(\omega t)]V_0, \tag{12}$$

where

$$H_0 = H_Z + H_X, \quad V_0 = H_Z - H_X, \tag{13}$$

$$H_Z = \sum_{i<j} J_{ij} Z_i Z_j + \sum_i h_i Z_i, \quad H_X = g \sum_i X_i. \tag{14}$$

Equivalently, the dynamics are governed by the Floquet unitary

$$U_F = e^{-i\frac{H_Z T}{2}} e^{-iH_X T} e^{-i\frac{H_Z T}{2}}, \tag{15}$$

where $T = \frac{2\pi}{\omega}$ is the period of the drive. We take the couplings to be random variables and average over realizations. For each realization, the $\frac{N(N-1)}{2}$ couplings J_{ij}, and the N longitudinal fields h_i, are first sampled from a standard normal distribution, then shifted and scaled such that

$$\langle J_{ij}\rangle = \langle h_i\rangle = 0 \text{ and } \frac{1}{2}\langle J_{ij}^2\rangle = \langle h_i^2\rangle = \frac{1}{N}. \tag{16}$$

The transverse field is $g = 1$ unless otherwise stated. At strict infinite temperature ($\rho \propto I$), this model satisfies $\langle H_Z^2\rangle = \langle H_X^2\rangle = N$.[4]

We choose to study this all-to-all quantum dot model because the main effects we are examining involve long timescales that are beyond what the Thouless time would be in an alternative geometrically local model, so on the relevant timescales those systems would also behave effectively as a quantum dot. Thus, the lack of geometric locality in our model is not important. We also use a square-wave drive to make the Floquet unitary easier to construct numerically. We do not expect the higher harmonics present in the Fourier spectrum of the square wave to play a significant role due to the exponential dependence on frequency of the relevant matrix elements and rates discussed earlier.

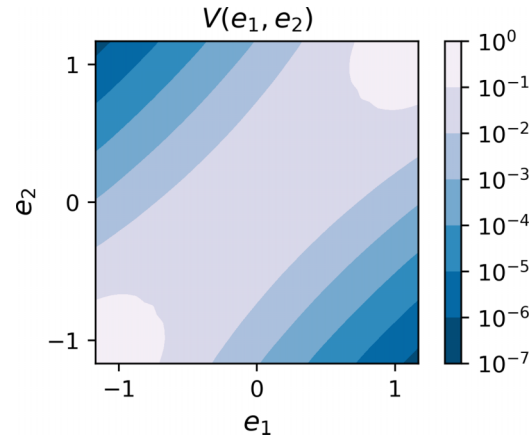

FIG. 3. Matrix elements of V_0 between eigenstates of H_0 at different energy densities. $V(e_1, e_2)$ is obtained by averaging the absolute value of the matrix elements over states and samples. These data are for samples with $N = 14$ qubits.

In Fig. 3 we show contours of $V(e_1, e_2)$ for our model system with $N = 14$ qubits. The evenly spaced, rather straight, contours indicate the expected exponential suppression in ω, and a weak dependence of $f(\Delta e, \bar{e})$ on $\bar{e}$.

A. Floquet thermalization when $e_2 = -e_1 = \frac{\Delta e}{2}$

As the most straightforward case of a crossover between the phases discussed in Sec. II C, and shown in Fig. 2, we take $e_2 = -e_1$ and tune $\Delta e = \omega/N$ to see when the thermalization across zones (Floquet heating) turns on or off. In this case $D(e_1) = D(e_2)$ and we imagine a system initialized at energy density $e_1 = -\frac{\Delta e}{2}$ and driven at frequency $\omega = N\Delta e$. In order to determine if the system will exchange energy with the drive and equally populate states at $e_2 = +\frac{\Delta e}{2}$ in its final

[4]Without the h_i fields we would have $\langle H_Z\rangle = N - 1$, so we include them to reduce this potential source of finite-size effects. These terms also break the Ising symmetry.

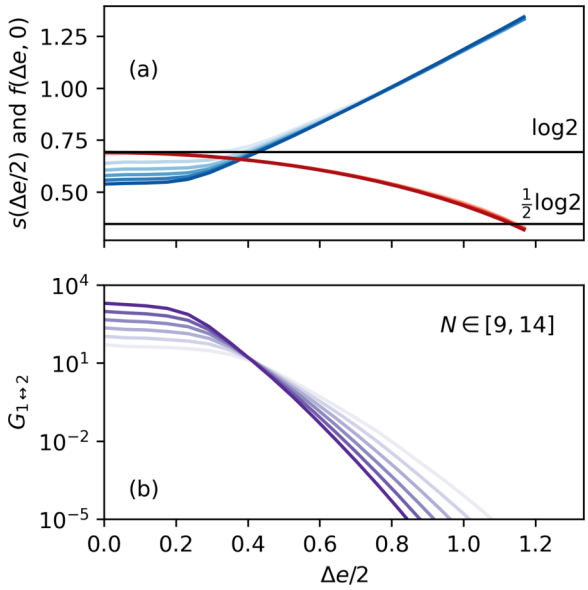

FIG. 4. Crossover between Floquet thermalization and energy localization along $e_2 = -e_1 = \frac{\Delta e}{2}$: linear response. (a) The entropy density s and a slice of the matrix element scaling function f for $e_2 = -e_1 = \frac{\Delta e}{2}$. s is shown in red and f in blue. System sizes N are 9–14 (light to dark). The horizontal black lines are the $N \to \infty$ expectations $s(0) = \log 2$ and $f(0, 0) = \frac{\log 2}{2}$ from random matrix theory. The right edge of the plot corresponds to the realization-averaged edge of the spectrum. (b) The quantity $G_{1\leftrightarrow 2} = V_{12}^2 D_1 D_2$ for the same data as (a).

equilibrium, i.e., becomes delocalized in energy, we want to test the condition (6). Note that the equality of the DOS at e_1, e_2 means that there is no one-way thermalization phase to discuss for this line cut through the phase diagram. We test the condition (6) in the two following ways:

First, we include finite-size corrections to Eqs. (3) and (4) (see Appendix B), and extract $s(\frac{\Delta e}{2})$ and $f(\Delta e, 0)$ from data at $N \in [9, 14]$. When these two quantities cross, that indicates a change in the condition of Eq. (6). The result is shown in Fig. 4(a). There we see a crossover at $\frac{\Delta e}{2} \approx 0.4$ at large N. This corresponds to $\omega \approx 0.8N$. For context, the energy difference between the ground state and highest excited state is, on average, $\omega \approx 2.7N$ so energy localization sets in at frequencies significantly less than the many-body bandwidth. The main finite-size effect appears to be the existence of a flat region of width $\propto \frac{1}{N}$ in $f(\Delta e, 0)$ near $\Delta e = 0$. This is simply the width $O(1)$ window of frequencies, for which a photon can be absorbed by $O(1)$ degrees of freedom in $O(1)$ time, that exists before the widely studied exponential-in-ω dependence is incurred, and we can also see this plateau in the middle of Fig. 3.

Second, we consider the related, but more direct, quantity

$$G_{1\leftrightarrow 2} = V(e_1, e_2)^2 D(e_1) D(e_2). \tag{17}$$

This quantity corresponds to the condition (6) in that $G_{1\leftrightarrow 2}$ increases (decreases) exponentially with N when the condition is met (not met), modulo finite-size corrections to Eqs. (3) and (4). In Fig. 4(b), we directly compute the quantity $G_{1\leftrightarrow 2}$ for various system sizes. The finite-size crossings indeed appear to be consistent with our earlier analysis shown in Fig. 4(a), and some drift is expected due to the aforementioned finite-size effects.

An independent way to corroborate the existence of this sharp crossover between the two-way Floquet thermalizing phase and the energy-localized phase with only isolated resonances (see Fig. 2 along the line $e_2 = -e_1$ where the one-way phase vanishes) is to examine the eigenstates of the Floquet operator U_F near $\theta = \pi/T$, which corresponds to the ladder of energy densities $e \in [\ldots, -\frac{\omega}{2N}, +\frac{\omega}{2N}, \ldots]$ that we have been considering. Note that since $\omega \propto N$, the number of rungs on the ladder is finite and constant in N. In the phase where the system freely (but slowly) exchanges energy with the drive, the eigenstates of U_F will have energy distributions that have weight on all rungs of the energy ladder, with the weight on each rung set by the density of states there (as in Fig. 1). In contrast, when the system cannot Floquet thermalize, the eigenstates will be well localized (in energy) on a single rung. As a measure of this crossover we compute the entropy of the sign of the energy,

$$S_{\text{sign}} = -P_- \log_2(P_-) - P_+ \log_2(P_+), \tag{18}$$

for eigenstates of U_F with eigenvalue near -1 ($\theta = \pi/T$), where $P_\pm$ is the probability of $\text{sgn}(E) = \pm 1$. This quantity tends to zero in the energy-localized phase, and to one bit for states at quasienergy $\theta = \pi/T$ in the two-way Floquet thermalizing phase. In Fig. 5(a) we show the distribution of energy density for the Floquet eigenstate closest to $\theta = \pi/T$ in a single sample of U_F at $\omega = 0.8N$. The sign entropy is shown in Fig. 5(b), where we again see a finite-size crossing near $\frac{\Delta e}{2} \approx 0.4$ at accessible sizes, consistent with the picture developed around Fig. 4.

Note that the widths of the peaks in Fig. 5(a) are not set by the thermalization rate Γ, as in Fig. 1, because we are using H_0 rather than the optimal local H_{eff} here (Appendix A). The peaks can be made much narrower by including corrections to H_0 [67].

Finally, in Fig. 6 we further examine the distribution of energy density in Floquet eigenstates at $\theta = \pi/T$ as we tune $\Delta e = \omega/N$: In Fig. 6(a) we plot the cumulative distribution function (CDF) of e for $\Delta e \in [0.36, 1.29]$. This range of Δe is chosen to span the infinite-temperature regime, the regime of the ladder ensemble, and the energy-localized regime. Importantly, we average over 10 samples and the 10 states closest to $\theta = \pi/T$ in each sample. However, for each state, we artificially flip the sign of the energy e so that there is more weight on $e < 0$ than $e > 0$. We do this so that we do not generate averaged energy distributions that are symmetric about $e = 0$ by averaging over states and samples, which would hide the trace of energy localization. In Fig. 6(a), we see that at low frequencies the distribution follows an infinite-temperature curve; at moderate frequencies the distribution is still balanced about $e = 0$, but is peaked at positive and negative e and not $e = 0$, characteristic of the ladder ensemble; at high frequencies the distribution becomes imbalanced about $e = 0$, indicating energy localization. In the lower panel, Fig. 6(b), we show the value of the CDF at $e = 0$ in red, and the probability density function (PDF) at $e = 0$ normalized by the infinite-temperature ($\beta = 0$) value in blue. We compute the PDF as the slope of the CDF. In that panel we see that the PDF at $e = 0$ begins to be reduced

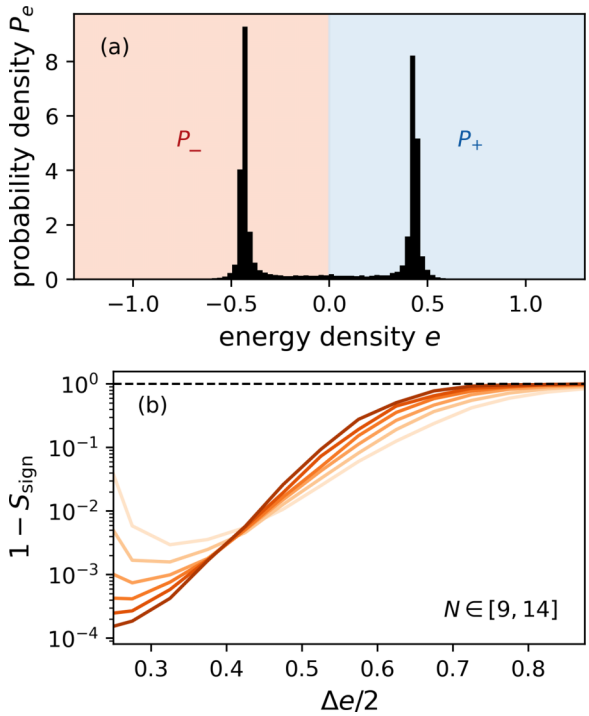

FIG. 5. Crossover between Floquet thermalization and energy localization along $e_2 = -e_1 = \frac{\Delta e}{2}$: full Floquet dynamics. (a) An example of the probability distribution P_e over energy density (with respect to H_0), for the eigenstate of U_F closest to $\theta = \pi/T$ in a single sample with $N = 13$ and $\Delta e = 0.8$. The shaded red and blue halves indicate the probability of the sign $P_\pm$. (b) The complement of the entropy of the sign of the energy. The result is averaged over samples of U_F and the two eigenstates on either side of $\theta = \pi/T$ within each sample. System sizes $N = 9$–14 correspond to light to dark curves.

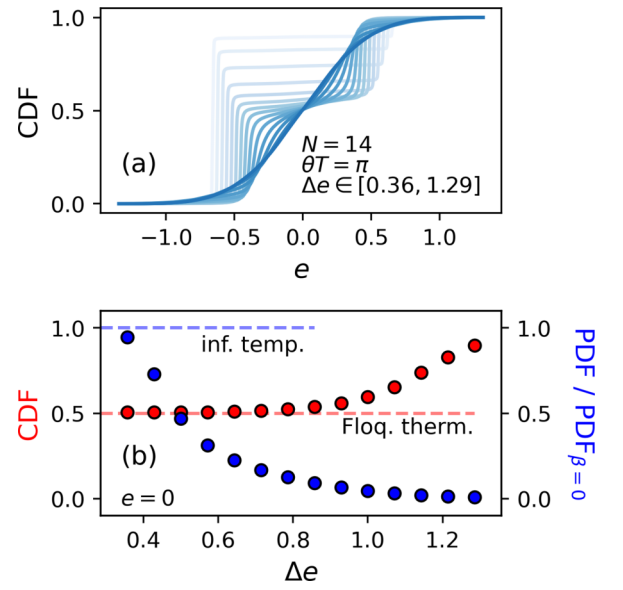

FIG. 6. Distributions of energy density in Floquet eigenstates at $\theta = \pi/T$. (a) The cumulative distribution function (CDF), averaged over 10 samples of U_F and 10 eigenstates near $\theta = \pi/T$ in each sample. We flip the sign of e as needed for each state before averaging over states so that if the states are imbalanced in energy, the average over states is too. $\Delta e \in [0.36, 1.29]$ are evenly spaced and correspond to dark-to-light curves. All data are for $N = 14$ qubits. (b) The CDF (red) and normalized probability density function (PDF) (blue) at $e = 0$. The CDF at $e = 0$ takes a value $\frac{1}{2}$ (dashed red line) when the distribution is balanced about $e = 0$. This happens when the system Floquet thermalizes. The normalized PDF at $e = 0$ takes the value 1 (dashed blue line) when the system thermalizes to the featureless infinite-temperature ensemble.

relative to the infinite-temperature value already at $\Delta e \approxeq 0.4$ (for $N = 14$), whereas the CDF deviates from the balanced value of $\frac{1}{2}$ around $\Delta e \approxeq 0.8$, in agreement with our earlier finding that energy localization begins to set in near that point (Figs. 4 and 5). This demonstrates that even in small numerically accessible systems of size $N = 14$ the regimes of applicability for the infinite-temperature and ladder ensembles are distinguishable: Floquet thermalization to the ladder ensemble extends significantly beyond the regime in which the system thermalizes to a featureless infinite-temperature state.

B. Floquet heating the ground state

Another scenario of interest is one where the system is initialized in the ground state of H_0, and driven at a frequency $\omega = N\Delta e$ so as to potentially cause heating to higher energy densities ($e_1 = e_{\text{gs}}$ and $e_2 = e_{\text{gs}} + \Delta e$). Here, too, there is a sharp "heating crossover," in the limit of large N, as a function of Δe, but it is of a slightly different nature than the earlier case of $e_2 = -e_1 = \frac{\Delta e}{2}$. In this crossover, the ground state will not serve as a continuum to transition to, from higher-energy densities, because of its vanishing entropy density, so the question is whether or not states at e_2 appear to be a continuum to the ground state at e_1. This question is closely related to the very recently investigated "Emergence of Fermi's Golden Rule" [66], where a single state coupled to a pseudocontinuum produced by a finite system was considered. The corresponding crossover is from the one-way Floquet thermalizing phase directly to the energy-localized phase with no resonances, so in Fig. 7(a) we examine the quantity

$$G_{1\to 2} = V(e_1, e_2)^2 D(e_2)^2, \tag{19}$$

which corresponds to, e.g., the right-side condition in Eq. (8). There we see an indicated crossover, which sharpens up with increasing N, at about $\Delta e \approxeq 0.96$ for the largest system sizes we can access. We also note that the quantity $G_{1\to 2}$ corresponds [up to an $O(1)$ factor] to the quantity γ from Ref. [66], which is the unitless tuning parameter of a universal scaling function for the emergence of FGR. That emergence occurs over an $O(1)$ scale in $\log\gamma \sim 2[\log V(e_1, e_2) + \log D(e_2)] \propto N$, consistent with the aforementioned statement that the width of the crossovers at $\omega \propto N$ studied in this work are asymptotically $\propto N^{-1}$.

Again as an independent check of the sharpening crossover in Fig. 7(a), we also compute the probability that the ground state of H_0 will remain indefinitely within the initial Floquet zone under the full dynamics of U_F. We define the boundary of the ground state's Floquet zone as $E = E_{\text{gs}} + \frac{\omega}{2}$. This is shown in Fig. 7(b), and we see that there is a finite-size crossing in agreement with our analysis of $G_{1\to 2}$.

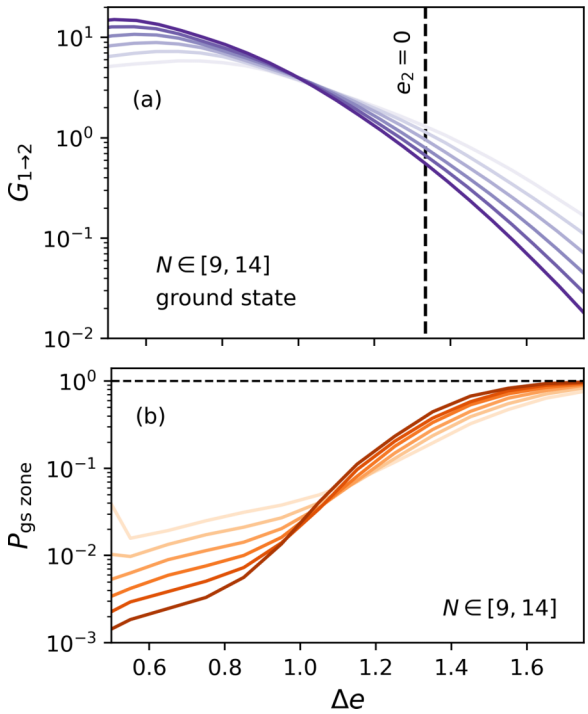

FIG. 7. Ground-state heating crossover. (a) The quantity $G_{1\to 2}$ (see main text) indicating the validity of Fermi's golden rule for heating from the ground-state energy density $e_1 = e_{\text{gs}}$ to $e_2 = e_{\text{gs}} + \Delta e$. Darker curves correspond to larger N. The vertical dashed line marks the point at which e_2 is at the center of the spectrum. The horizontal axis is shared with the bottom panel. (b) The probability that the ground state of H_0 stays within its Floquet zone ($e \in [e_{\text{gs}}, e_{\text{gs}} + \frac{\Delta e}{2}]$) indefinitely, under time evolution by U_F.

C. The full phase diagram

So far, we have considered two cuts through the full (e_1, e_2) plane, and examined the crossovers that occur along them while the (extensive) frequency of the drive is tuned. These crossovers separate different degrees of thermalization that can occur in Floquet systems. We now expand our analysis to the full two-dimensional (2D) phase diagram in this plane, with all of the phases discussed in Sec. II. A notable feature of the phase diagram is the strong dependence of phase boundaries on the Floquet quasienergy (set by e_1, e_2), an issue that is mostly ignored in conventional studies of Floquet systems that typically do not explore the dependence on quasienergy.

The phase diagram is shown in Fig. 2. The solid lines and dots on that diagram are obtained using only the $N \in \{12, 14\}$ data, and the dashed lines are sketched extrapolations. The boundary between the phases with two-way and one-way Floquet thermalization marks the point at which $G_{1\leftrightarrow 2}$ goes from increasing with N to decreasing. (For the curves in Fig. 2, the range of N we use to determine whether a quantity is increasing or decreasing with N contains only $N = 12$ and 14.) Similarly, the boundary between the one-way Floquet thermalizing phase and the energy-localized phase with isolated resonances marks where $G_{1\to 2}$ goes from increasing to decreasing with N. The union of the two-way and one-way phases is where full or partial interzone thermalization occurs, e.g., Floquet heating, so the blue boundary in Fig. 2 is the most experimentally relevant. The middle and edge of this boundary are the crossovers observed in Figs. 4 and 7. Lastly, the boundary between having isolated resonances and not having Floquet resonances is marked by the quantity $G_r = V(e_1, e_2)D(e_1)D(e_2)$ increasing and decreasing, respectively, with N because G_r corresponds to the condition on the right side of Eq. (10). As mentioned earlier, the curves in Fig. 2 will drift with system size, but an understanding of the qualitative organization of the phases is what we are trying to achieve here.

IV. EXPERIMENTAL CONSIDERATIONS

Since one inspiration for our work is that many experimental platforms for exploring isolated quantum many-body physics are mesoscopic in size, in this section we discuss some experimental considerations and simulate an experiment that could be performed on such small near-term platforms.

Ideally (in theory), we are studying features of systems that occur at large N-dependent drive frequencies. Floquet thermalization rates (when Floquet thermalization does occur) at those frequencies are exponentially suppressed in $\omega \propto \Omega(N)$, where $\Omega(N)$ is an increasing function of N, and this slowness is one of the main obstacles for any experimental realizations of the physics discussed in this work. However, as we show in this section, for small systems it may be possible to observe some nontrivial phenomena on experimentally realistic timescales. Other obstacles for potential experiments are that the resolution with which the energy distribution can be probed can be limited by both the initial states that can be prepared and the type of measurements that are possible. Platforms with an intermediate number (tens) of qubits, atoms, ions, etc., long coherence times (in units of the relevant interaction time), and "site-resolved" measurement capabilities would be the most appropriate for experimental explorations of some of the physics presented in this paper.

As an example, here we explore the specific goal of probing the kind of ladderlike Floquet thermal equilibrium shown in Figs. 1(c) and 5(a), where the average energy density corresponds to infinite temperature, but the system actually relaxes to a linear combination of positive and negative temperature states, with almost no weight on states with zero energy density, a situation quite different from the conventional featureless infinite-temperature ensemble. For the purpose of demonstration, we continue to use the N-qubit model detailed in Sec. III.

The system must be in the Floquet thermalizing phase for this to work, so first we choose a value for $\Delta e = \frac{\omega}{N}$ such that the system will eventually exchange energy with the drive. The initial state will be a pure state with energy density $-\frac{\Delta e}{2}$, and must have energy density uncertainty $\ll \Delta e$. We then allow the system to evolve for long enough times that Floquet thermalization occurs and the system populates a ladder of distinct energy densities. In this situation, while $\langle H_0 \rangle / N$ converges to zero, the variance of the energy density is $O(1)$ rather than $\propto \frac{1}{N}$, as is the case in the featureless infinite-temperature ensemble. Ideally, this can be observed via few-body energy-density

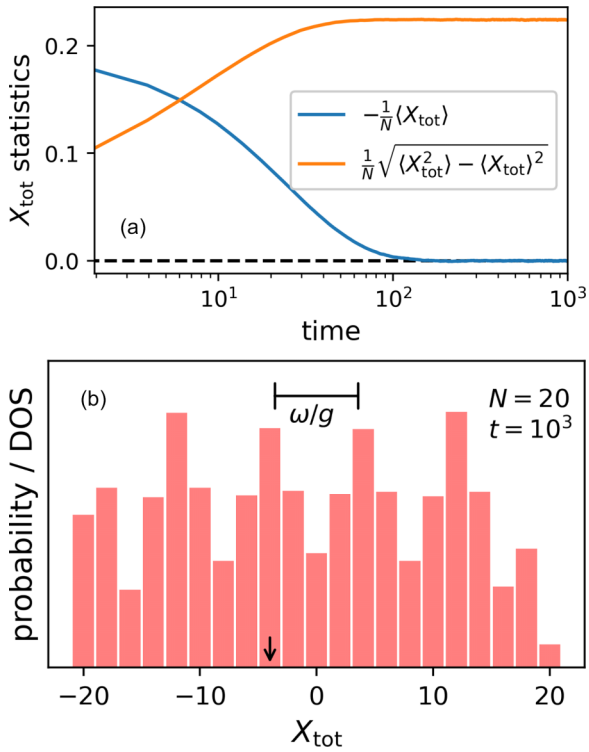

FIG. 8. The distribution of measurements of $X_{\rm tot}$. The data are for one sample of the system described in the main text of Sec. IV, with $N = 20$. (a) The time evolution of the (negative) mean and standard deviation of $X_{\rm tot}/N$. Time is measured in microscopic units, not Floquet cycles. (b) The full distribution of outcomes when measuring $X_{\rm tot}$ at time $t = 10^3$. The initial state is an eigenstate of $X_{\rm tot}$ with eigenvalue indicated by the small black arrow.

correlations; some variation of the system size would be needed in order to differentiate a small $O(1)$ value from a value that is vanishing with N. However, a simpler protocol would be of more practical value, and that is what we discuss below.

Projectively measuring the global energy H_0 is not realistically possible, so the distribution of H_0 (not to mention some ideal $H_{\rm eff}$) cannot be probed exactly. However, if a substantial part of the Hamiltonian can be measured, e.g., $H_X = g\sum_i X_i$ in our model (see Sec. III), then this simple piece can act as a good proxy for the global energy in some respects. For example, in our model, extensive energy fluctuations can be detected through long-range XX correlations in the system. Better yet, one can look at the full distribution ("full counting statistics" [72–75]) of measurement outcomes of the total X magnetization $X_{\rm tot} = \sum_i X_i$, which is a realistic observable in many platforms that can take simultaneous snapshots of all degrees of freedom in the system. (Alternatively, one could measure all Z operators and thus look at that component of the energy. But we will focus on the X part of the energy since one-qubit operators can generally be measured with higher fidelity.)

The above discussion suggests that we should set $g > 1$ so that H_X is a larger component of H_0, so here we set $g = 2$, which turns out to be sufficient for the present purposes. We consider the unitary evolution of the initial pure state $|\psi(0)\rangle = |+\rangle^{N_+}|-\rangle^{N-N_+}$, i.e., N_+ qubits in the $X = +1$ state and $N - N_+$ in the $X = -1$ state. This initial state has energy density $e_1 = -g(1 - \frac{2N_+}{N})$ and energy density uncertainty $\frac{1}{\sqrt{N}}$ (the prefactor is 1). We drive the system at frequency $\omega = 2N|e_1|$ to induce transitions to $e_2 = -e_1$ and other energies in the "ladder." In Fig. 8 we show data for a system with $N = 20$ qubits, initialized in the aforementioned state with $N_+ = 8$, and driven at the frequency $\omega = 16$. Importantly, this frequency is not so large that we should worry about coupling the state space of the idealized model to other "nonmodel" states that would exist in a real experimental system. For the above values of N, N_+, and ω, the initial state has $\frac{\sigma_E}{2|E|} \approx 0.28$, so we can hope to resolve an energy-ladder-like equilibrium at long times by measuring X_i on all of the qubits simultaneously. We limit ourselves to the times $t \leqslant 10^3$ so as to not require times far beyond what may be experimentally feasible on near-term platforms. Figure 8(a) shows the time evolution of the mean and standard deviation of $X_{\rm tot}$, both normalized by N based on the expectation of extensive fluctuations. Figure 8(b) shows the full quantum distribution, at $t = 10^3$, of $X_{\rm tot}$ normalized by the DOS of $X_{\rm tot}$, so that the state $\rho \propto I$ would result in a flat graph. The distribution clearly shows a ladder of spacing $\frac{\omega}{g}$ that develops, which corresponds to an energy ladder of spacing ω.

From the above numerical experiment, we conclude that some aspects of the more complete description of Floquet thermalization that we have provided in this work should be experimentally accessible on near-term quantum simulation platforms.

V. SUMMARY AND DISCUSSION

In this paper we present a more complete picture of Floquet thermalization and its absence in many-body quantum systems than was previously established, thus advancing our understanding of fundamental aspects of isolated periodically driven systems. By allowing the drive frequency ω to scale up with N, we identify a variety of phases, separated by crossovers that sharpen as $N \to \infty$; these are representative of different regimes of thermalization that can be present in mesoscopic Floquet systems. We find a different Floquet thermal ensemble, the ladder ensemble, which is qualitatively distinct from the featureless infinite-temperature state that is achieved in the conventionally studied case where ω remains finite as $N \to \infty$. In fact, we show that the conventional infinite-temperature ensemble is valid only in a vanishing fraction of the phase diagram where Floquet thermalization does occur. Thus, we show that Floquet thermalization does *not* imply that the system thermalizes to infinite temperature, even on average. Two of the phases we detail host full or partial Floquet thermalization (delocalization in energy), but their equilibrium distribution over energy is qualitatively different from an infinite-temperature state. The other two phases fail to Floquet thermalize and thus are localized in energy, but are distinguished by the presence or absence of rare Floquet many-body resonances in typical samples. We present a phase diagram delineating these various regimes, and the phase boundaries show strong dependence on Floquet quasienergy, or the energy of an initial state, a feature that is mostly ignored in conventional studies.

We also explored the feasibility of experimentally observing our findings, and found that some interesting types of Floquet thermalization elucidated in this work should be realizable on near-term quantum simulation platforms. In particular, we simulated an experiment in which a small Floquet system thermalizes on an accessible timescale to a superposition of thermal states at a set of evenly spaced and extensively different energies.

One of our primary motivations for studying Floquet thermalization in mesoscopic systems is that many physically relevant settings only have access to small or moderate-size systems, and our theoretical understanding of thermalization and equilibrium in this setting is still quite incomplete, as illustrated by our findings. These settings include numerical experiments limited to small sizes, and experiments on near-term quantum simulators operating in the intermediate-scale regime [56]. For example, recent works have studied Trotter approximations for digital quantum simulation [76–78], and identified thresholds as a function of the Trotter step size separating regimes with controllable and uncontrolled Trotter errors. These Trotterization protocols are simply Floquet evolutions with frequency controlled by the step size, and our work elucidates the theoretical basis behind these topical studies: the observed thresholds are simply Floquet heating thresholds that occur at an extensive frequency, $\omega \propto N$, a scaling that was not identified in these works.

A second motivation for our work draws on the fact that finite-size and finite-time crossovers between fully and partially or nonthermalizing regimes have become increasingly important in a number of contexts, most notably in the study of many-body localization, but also in, e.g., integrability breaking [55]. Here, recent work has led to the understanding that the numerically and experimentally observed crossovers between thermalizing and MBL-like regimes have distinct physics from that of the asymptotic phase transition [69,79,80]. Indeed, an MBL-to-thermal phase transition may not even exist in the standard thermodynamic limit in higher dimensions or with power-law interactions, even though a crossover is clearly observed in these settings [52–54,81]. Understanding the universal properties of such crossovers is an important open question, and our hope is that developing a more complete theory of the finite-size crossovers associated with the onset of Floquet heating and rare Floquet resonances will also prove illuminating for these other, arguably more challenging, cases.

We note that the crossovers we have studied in this work are examples of boundaries between different types of thermal phases since even the energy-localized phase is described by a chaotic H_{eff}. In contrast, the relevant processes for crossovers into or between many-body localized regimes have extremely broadly distributed matrix elements that may need to be taken in to account [69,71]. Nonetheless, both Floquet thermalization crossovers studied in this work, and the observable crossover between thermal and MBL regimes, have some similarities. For example, these crossovers have *apparent* critical exponents $\nu \cong 1$. In the case of Floquet thermalization (setting some factors to 1 for brevity) this is a result of the interzone relaxation time $\Gamma^{-1} \sim e^{\omega} = e^{(\omega/N)N}$ passing through the relevant Heisenberg time $\tau_{\text{H}} \sim e^{sN}$ as a function of the control parameter ω/N, as discussed above. In the case of the numerically observable MBL crossover, the apparent $\nu \cong 1$ in finite-size systems is similarly a result of a thermalization time that behaves as $\sim e^{k(W)N}$ near the crossover [69,79,80,82–85] passing through the Heisenberg time as a function of the control parameter W. It may be that understanding the simpler cases of thermal-to-thermal crossovers, as we have done in this work, will provide some insights that are helpful for addressing the more challenging situations where the crossover involves nonthermal states.

In future studies it would be interesting to realize some of the phenomenology explored in this work experimentally, as we have shown that it should be within reach of some current experimental platforms for quantum simulation. It would also be interesting to consider Floquet systems where H_0, the time-averaged Hamiltonian, is not fully chaotic, as an intermediate problem where the energy-localized phase may thermalize only asymptotically slowly, or not at all. Another interesting direction is to consider an H_0 with quantum scars to explore the thermalization of the scar state across Floquet zones as a function of the drive frequency and energy of the scar state. Further studies of the dynamics throughout the phase diagram that we have mapped out here would also be interesting, as our work is primarily concerned with the final equilibrium that is achieved. Finally, many of our findings should have analogs in static settings where, for example, a system is governed by a Hamiltonian $\hat{H} = \hat{K} + \Delta\hat{M}$, where $\hat{M}$ has an integer spectrum, Δ is a large parameter, and $\hat{K}$ couples states within and across eigenspaces of $\hat{M}$ [41]. Examples of such settings include systems with a weakly broken U(1) symmetry corresponding to conservation of total charge, or scarred Hamiltonians derived from parent Hamiltonians with a spectrum generating algebra [86–88], or systems with approximate Hilbert space fragmentation due to weakly broken conservation of charge and dipole moment [89,90].

ACKNOWLEDGMENTS

We thank I. Bloch, V. Bulchandani, A. Chandran, S. Garratt, S. Gopalakrishnan, A. Polkovnikov, M. Rigol, D. Wei, and J. Zeiher for helpful discussions and/or previous collaborations. A.M. was supported in part by the DARPA DRINQS program, the Stanford Q-FARM Bloch Postdoctoral Fellowship in Quantum Science and Engineering, and the Gordon and Betty Moore Foundation's EPiQS Initiative through Grant No. GBMF8686. D.A.H. and A.M. were supported in part by NSF QLCI Grant No. OMA-2120757. V.K. was supported by the U.S. Department of Energy, Office of Science, Basic Energy Sciences, under Early Career Award No. DE-SC0021111, the Alfred P. Sloan Foundation through a Sloan Research Fellowship, and the Packard Foundation through a Packard Fellowship in Science and Engineering. Simulations presented in this work were performed on computational resources managed and supported by Princeton Research Computing. We also acknowledge the hospitality of the Kavli Institute for Theoretical Physics at the University of California, Santa Barbara (supported by NSF Grant No. PHY-1748958).

APPENDIX A: THE EFFECTIVE HAMILTONIAN H_{eff}

In Sec. II we use the concept of an effective Hamiltonian H_{eff}. This is a concept that is helpful in discussions of Floquet prethermalization and thermalization, but in later sections we use H_0 as a sufficient definition of energy. Here we want to clarify the difference between H_{eff} and an approximation to it, like H_0.

A good H_{eff} is one that captures the processes that do not result in resonant transitions across Floquet zones, e.g., interzone transitions that are mediated by virtual transitions to other Floquet zones. A nearly optimal H_{eff} therefore approximates the dynamics of the system on timescales shorter than Γ^{-1}, the long timescale on which quanta of energy $\sim\omega$ are resonantly exchanged with the drive. For nearly optimal H_{eff} and large enough ω, $H_{\text{eff}}\text{mod}\omega$ will be approximately conserved for all times, up to a precision Γ (Fig. 1). For our considerations, we can think of H_{eff} as being "obtained" perturbatively until the series stops improving the approximation $\mathrm{e}^{-iH_{\text{eff}}T}\approx U_F$, although we do not actually need to have a strict definition of H_{eff} or a method for constructing it. The perturbative series is in the small parameter (J/ω), where J is a microscopic energy scale and it goes up to order $n\sim O(\omega/J)$. When $\omega/J\sim N$, there are terms with support on $O(N)$ qubits, but those terms are suppressed by coefficients that are $\sim[1/O(N)]^{O(N)}$. Due to this extreme suppression, as we scale ω up faster with N, the effective Hamiltonian gets *more* local, not less local, in the sense that all terms but H_0 go to zero in the limit of large N due to their coefficients vanishing.

Thus, for our purposes, using H_0 as a notion of energy in the system is sufficient due to the large overlap between H_0 and H_{eff}. H_0 is approximately conserved on timescales shorter than Γ^{-1}, too, but the precision of that approximate conservation law is not good enough for H_0 to describe the full dynamics of the system on long timescales because it does not capture the perturbative processes mediated by virtual transitions to other Floquet zones. Importantly, this means that the widths of the peaks of the distribution of H_0 in eigenstates of U_F will not be $\sim\Gamma$, but will be substantially broader due to intrazone dynamics that are captured by H_{eff} but not by H_0. More specifically, due to the correction $H_{\text{eff}}-H_0=\frac{1}{\omega}H_1+\cdots$, we expect an additional broadening of the energy peaks (in energy H_0) of $\sim\frac{\sqrt{N}}{\omega}$.

APPENDIX B: ESTIMATING $s(e)$ AND $f(\Delta e,\bar{e})$ FROM FINITE-SIZE DATA

Near $E=0$, where most of the spectral weight is, the density of states is Gaussian with variance $\sigma^2=2N$ (from Sec. III). Thus, we expect $D(0)=(4\pi N)^{-\frac{1}{2}}\mathrm{e}^{N\log 2}$ and so we extract s from small-N numerical data via

$$s\left(\frac{\Delta e}{2}\right)=\frac{1}{N}\log\left[\sqrt{4\pi N}D\left(\frac{\Delta e}{2}\right)\right]. \tag{B1}$$

For the matrix elements, we assume the form $V(-\frac{\Delta e}{2},\frac{\Delta e}{2})=A\mathrm{e}^{-Nf(\Delta e,0)}$ and take the N and Δe dependence of A [1] to be subleading within the small window of N we have data for. Thus, we extract f from numerical data via

$$f(\Delta e,0)=-\frac{1}{N}\log\left[\frac{1}{A}V\left(-\frac{\Delta e}{2},\frac{\Delta e}{2}\right)\right], \tag{B2}$$

and fit A in order to collapse the data beyond $\Delta e\sim\frac{1}{N}$ $[\omega\sim O(1)]$.

APPENDIX C: THE TWO-ZONE APPROXIMATION

The Floquet thermalization and resonances phase diagram of Fig. 2 was generated using the two-zone approximation. In this approximation we are ignoring the Floquet zones outside of the two being considered (at energy densities e_1 and e_2). Minor quantitative modifications to the phase diagram can occur due to considering the other zones. The concern is that, when considering the point (e_1,e_2), if there is another e_3 in the energy ladder that has a larger density of states than e_1 and e_2, it may be relevant. More specifically, if (e_1,e_2) is in the one-way Floquet thermalization phase, and e_3 has a larger density of states and (e_2,e_3) are in the two-way phase, then we should update the DOS of e_2 to include the states at e_3, and that may cause (e_1,e_2) to become part of the two-way phase.

We will first state which areas of the phase diagram are completely safe from the influence of extra zones, i.e., the rest of the energy ladder. Since the phase diagram is symmetric, we consider the tile that has positive Δe and negative $\bar{e}$ (see Fig. 2), so $D(e_1)<D(e_2)$. Now as long as $e_2\in[-\frac{\Delta e}{2},\frac{\Delta e}{2}]$, then it is the rung in the ladder with the highest density of states. This means that the phase diagram (in the tile considered) could only be modified by third-zone effects below the line $e_2=\frac{e_1}{3}$.

But this region can be constrained even further because the danger comes from other pairs of rungs in the ladder that are in the two-way phase. Thus, a line of constant Δe that is tangent to the top of the two-way phase also bounds the region of concern.

From these considerations, we can deduce that the two-way phase may bulge out into the one-way phase a little more than is shown in Fig. 2 in the lower left and upper right corners of that phase diagram, but that is all that can be modified by going beyond the two-zone approximation.

APPENDIX D: FINITE-TIME FLOQUET THERMALIZATION CROSSOVER IN INFINITE SYSTEMS

For completeness, in this Appendix we note a few aspects of the Floquet thermalization crossover that occur in systems of effectively infinite size when tuning the drive frequency ω and observing at fixed time t. Large enough systems do eventually thermalize to infinite temperature (see Sec. II), and the energy density changes at a rate $\Gamma\sim\mathrm{e}^{-\omega/\omega_0}$. As we increase ω, most of the heating that occurs in the system will go from happening before time t to after time t. Thus, a crossover in the energy density e at time t will occur, and here we show that this crossover sharpens in a sense as the observation time t is increased.

Consider a system initialized with $e=O(-1)$ energy density and driven to heat up to $e=0$ eventually. We have a fixed observation time t and our tuning parameter is ω.

The change in the energy density by the observation time is $\delta e(\omega) \sim t e^{-\omega/\omega_0}$ as long as the heating is far from complete. This hits a set threshold value when $\omega \sim \omega_0 \log t$. The width of the crossover through that threshold value is

$$\left| \frac{d\delta e}{d\omega}\bigg|_{\omega=\omega_0 \log t} \right|^{-1} \sim \omega_0. \tag{D1}$$

Therefore, the width of the Floquet thermalization crossover is down by a factor of $\log t$ from the location of the crossover, and this means that the crossover sharpens up logarithmically as a function of increasing observation time t.

If we exit the regime where N is effectively infinite and allow the observation time to approach the inverse many-body level spacing of the system, then $\log t \propto N$ so the crossover sharpens linearly in N. This is consistent with statements in the main text that the width of the crossovers (in ω/N) shown on the phase diagram scale as N^{-1}.

[1] L. D'Alessio, Y. Kafri, A. Polkovnikov, and M. Rigol, From quantum chaos and eigenstate thermalization to statistical mechanics and thermodynamics, Adv. Phys. **65**, 239 (2016).

[2] R. Nandkishore and D. A. Huse, Many-body localization and thermalization in quantum statistical mechanics, Annu. Rev. Condens. Matter Phys. **6**, 15 (2015).

[3] D. A. Abanin, E. Altman, I. Bloch, and M. Serbyn, Colloquium: Many-body localization, thermalization, and entanglement, Rev. Mod. Phys. **91**, 021001 (2019).

[4] F. Alet and N. Laflorencie, Many-body localization: An introduction and selected topics, C. R. Phys., **19**, 498 (2018).

[5] M. Serbyn, D. A. Abanin, and Z. Papić, Quantum many-body scars and weak breaking of ergodicity, Nat. Phys. **17**, 675 (2021).

[6] S. Moudgalya, B. A. Bernevig, and N. Regnault, Quantum many-body scars and hilbert space fragmentation: A review of exact results, Rep. Prog. Phys. **85**, 086501 (2022).

[7] A. Chandran, T. Iadecola, V. Khemani, and R. Moessner, Quantum many-body scars: A quasiparticle perspective, Annu. Rev. Condens. Matter Phys. **14**, 443 (2023).

[8] R. V. Jensen and R. Shankar, Statistical behavior in deterministic quantum systems with few degrees of freedom, Phys. Rev. Lett. **54**, 1879 (1985).

[9] J. M. Deutsch, Quantum statistical mechanics in a closed system, Phys. Rev. A **43**, 2046 (1991).

[10] M. Srednicki, Chaos and quantum thermalization, Phys. Rev. E **50**, 888 (1994).

[11] M. Rigol, V. Dunjko, and M. Olshanii, Thermalization and its mechanism for generic isolated quantum systems, Nature (London) **452**, 854 (2008).

[12] M. Srednicki, Thermal fluctuations in quantized chaotic systems, J. Phys. A: Math. Gen. **29**, L75 (1996).

[13] M. Srednicki, The approach to thermal equilibrium in quantized chaotic systems, J. Phys. A: Math. Gen. **32**, 1163 (1999).

[14] M. Rigol, Breakdown of thermalization in finite one-dimensional systems, Phys. Rev. Lett. **103**, 100403 (2009).

[15] M. Rigol, Quantum quenches and thermalization in one-dimensional fermionic systems, Phys. Rev. A **80**, 053607 (2009).

[16] W. Beugeling, R. Moessner, and M. Haque, Finite-size scaling of eigenstate thermalization, Phys. Rev. E **89**, 042112 (2014).

[17] H. Kim, T. N. Ikeda, and D. A. Huse, Testing whether all eigenstates obey the eigenstate thermalization hypothesis, Phys. Rev. E **90**, 052105 (2014).

[18] R. Mondaini, K. R. Fratus, M. Srednicki, and M. Rigol, Eigenstate thermalization in the two-dimensional transverse field ising model, Phys. Rev. E **93**, 032104 (2016).

[19] R. Mondaini and M. Rigol, Eigenstate thermalization in the two-dimensional transverse field ising model. II. Off-diagonal matrix elements of observables, Phys. Rev. E **96**, 012157 (2017).

[20] A. Lazarides, A. Das, and R. Moessner, Equilibrium states of generic quantum systems subject to periodic driving, Phys. Rev. E **90**, 012110 (2014).

[21] L. D'Alessio and M. Rigol, Long-time behavior of isolated periodically driven interacting lattice systems, Phys. Rev. X **4**, 041048 (2014).

[22] T. Prosen, Time evolution of a quantum many-body system: Transition from integrability to ergodicity in the thermodynamic limit, Phys. Rev. Lett. **80**, 1808 (1998).

[23] L. D'Alessio and A. Polkovnikov, Many-body energy localization transition in periodically driven systems, Ann. Phys. **333**, 19 (2013).

[24] P. Ponte, Z. Papić, F. Huveneers, and D. A. Abanin, Many-body localization in periodically driven systems, Phys. Rev. Lett. **114**, 140401 (2015).

[25] A. Lazarides, A. Das, and R. Moessner, Fate of many-body localization under periodic driving, Phys. Rev. Lett. **115**, 030402 (2015).

[26] V. Gritsev and A. Polkovnikov, Integrable Floquet dynamics, SciPost Phys. **2**, 021 (2017).

[27] P. W. Claeys and J.-S. Caux, Breaking the integrability of the heisenberg model through periodic driving, arXiv:1708.07324.

[28] A. Lazarides, A. Das, and R. Moessner, Periodic thermodynamics of isolated quantum systems, Phys. Rev. Lett. **112**, 150401 (2014).

[29] A. Russomanno, A. Silva, and G. E. Santoro, Periodic steady regime and interference in a periodically driven quantum system, Phys. Rev. Lett. **109**, 257201 (2012).

[30] V. Khemani, A. Lazarides, R. Moessner, and S. L. Sondhi, Phase structure of driven quantum systems, Phys. Rev. Lett. **116**, 250401 (2016).

[31] D. V. Else, B. Bauer, and C. Nayak, Floquet time crystals, Phys. Rev. Lett. **117**, 090402 (2016).

[32] C. W. von Keyserlingk, V. Khemani, and S. L. Sondhi, Absolute stability and spatiotemporal long-range order in Floquet systems, Phys. Rev. B **94**, 085112 (2016).

[33] K. Sacha and J. Zakrzewski, Time crystals: A review, Rep. Prog. Phys. **81**, 016401 (2018).

[34] V. Khemani, R. Moessner, and S. L. Sondhi, A brief history of time crystals, arXiv:1910.10745.

[35] M. S. Rudner, N. H. Lindner, E. Berg, and M. Levin, Anomalous edge states and the bulk-edge correspondence for periodically driven two-dimensional systems, Phys. Rev. X **3**, 031005 (2013).

[36] P. Titum, E. Berg, M. S. Rudner, G. Refael, and N. H. Lindner, Anomalous Floquet-Anderson insulator as a nonadiabatic quantized charge pump, Phys. Rev. X **6**, 021013 (2016).

[37] D. A. Abanin, W. De Roeck, and F. Huveneers, Exponentially slow heating in periodically driven many-body systems, Phys. Rev. Lett. **115**, 256803 (2015).

[38] T. Mori, T. Kuwahara, and K. Saito, Rigorous bound on energy absorption and generic relaxation in periodically driven quantum systems, Phys. Rev. Lett. **116**, 120401 (2016).

[39] T. Kuwahara, T. Mori, and K. Saito, Floquet-magnus theory and generic transient dynamics in periodically driven many-body quantum systems, Ann. Phys. **367**, 96 (2016).

[40] D. A. Abanin, W. De Roeck, W. W. Ho, and F. Huveneers, Effective Hamiltonians, prethermalization, and slow energy absorption in periodically driven many-body systems, Phys. Rev. B **95**, 014112 (2017).

[41] D. Abanin, W. De Roeck, W. W. Ho, and F. Huveneers, A rigorous theory of many-body prethermalization for periodically driven and closed quantum systems, Commun. Math. Phys. **354**, 809 (2017).

[42] A. Rubio-Abadal, M. Ippoliti, S. Hollerith, D. Wei, J. Rui, S. L. Sondhi, V. Khemani, C. Gross, and I. Bloch, Floquet prethermalization in a Bose-Hubbard system, Phys. Rev. X **10**, 021044 (2020).

[43] W. De Roeck and V. Verreet, Very slow heating for weakly driven quantum many-body systems, arXiv:1911.01998.

[44] D. J. Luitz, R. Moessner, S. L. Sondhi, and V. Khemani, Prethermalization without temperature, Phys. Rev. X **10**, 021046 (2020).

[45] W. W. Ho and W. De Roeck, A rigorous theory of prethermalization without temperature, arXiv:2011.14583.

[46] D. V. Else, B. Bauer, and C. Nayak, Prethermal phases of matter protected by time-translation symmetry, Phys. Rev. X **7**, 011026 (2017).

[47] A. Lerose, J. Marino, A. Gambassi, and A. Silva, Prethermal quantum many-body kapitza phases of periodically driven spin systems, Phys. Rev. B **100**, 104306 (2019).

[48] F. Machado, D. V. Else, G. D. Kahanamoku-Meyer, C. Nayak, and N. Y. Yao, Long-range prethermal phases of nonequilibrium matter, Phys. Rev. X **10**, 011043 (2020).

[49] M. Collura, A. De Luca, D. Rossini, and A. Lerose, Discrete time-crystalline response stabilized by domain-wall confinement, Phys. Rev. X **12**, 031037 (2022).

[50] D. V. Else, P. Fendley, J. Kemp, and C. Nayak, Prethermal strong zero modes and topological qubits, Phys. Rev. X **7**, 041062 (2017).

[51] B. L. Altshuler, Y. Gefen, A. Kamenev, and L. S. Levitov, Quasiparticle lifetime in a finite system: A nonperturbative approach, Phys. Rev. Lett. **78**, 2803 (1997).

[52] A. L. Burin, Many-body delocalization in a strongly disordered system with long-range interactions: Finite-size scaling, Phys. Rev. B **91**, 094202 (2015).

[53] K. S. Tikhonov and A. D. Mirlin, Many-body localization transition with power-law interactions: Statistics of eigenstates, Phys. Rev. B **97**, 214205 (2018).

[54] S. Gopalakrishnan and D. A. Huse, Instability of many-body localized systems as a phase transition in a nonstandard thermodynamic limit, Phys. Rev. B **99**, 134305 (2019).

[55] V. B. Bulchandani, D. A. Huse, and S. Gopalakrishnan, Onset of many-body quantum chaos due to breaking integrability, Phys. Rev. B **105**, 214308 (2022).

[56] J. Preskill, Quantum Computing in the NISQ era and beyond, Quantum **2**, 79 (2018).

[57] A. Morningstar, M. Hauru, J. Beall, M. Ganahl, A. G. M. Lewis, V. Khemani, and G. Vidal, Simulation of quantum many-body dynamics with tensor processing units: Floquet prethermalization, PRX Quantum **3**, 020331 (2022).

[58] K. Seetharam, P. Titum, M. Kolodrubetz, and G. Refael, Absence of thermalization in finite isolated interacting floquet systems, Phys. Rev. B **97**, 014311 (2018).

[59] X. Cao, A statistical mechanism for operator growth, J. Phys. A: Math. Theor. **54**, 144001 (2021).

[60] D. Sels and A. Polkovnikov, Thermalization of dilute impurities in one-dimensional spin chains, Phys. Rev. X **13**, 011041 (2023).

[61] D. E. Parker, X. Cao, A. Avdoshkin, T. Scaffidi, and E. Altman, A universal operator growth hypothesis, Phys. Rev. X **9**, 041017 (2019).

[62] K. Mallayya and M. Rigol, Heating rates in periodically driven strongly interacting quantum many-body systems, Phys. Rev. Lett. **123**, 240603 (2019).

[63] T. Mori, Heating rates under fast periodic driving beyond linear response, Phys. Rev. Lett. **128**, 050604 (2022).

[64] T. N. Ikeda and A. Polkovnikov, Fermi's golden rule for heating in strongly driven floquet systems, Phys. Rev. B **104**, 134308 (2021).

[65] A. Rakcheev and A. M. Läuchli, Estimating heating times in periodically driven quantum many-body systems via avoided crossing spectroscopy, Phys. Rev. Res. **4**, 043174 (2022).

[66] T. Micklitz, A. Morningstar, A. Altland, and D. A. Huse, Emergence of fermi's golden rule, Phys. Rev. Lett. **129**, 140402 (2022).

[67] M. Bukov, M. Heyl, D. A. Huse, and A. Polkovnikov, Heating and many-body resonances in a periodically driven two-band system, Phys. Rev. B **93**, 155132 (2016).

[68] M. Serbyn, Z. Papić, and D. A. Abanin, Criterion for many-body localization-delocalization phase transition, Phys. Rev. X **5**, 041047 (2015).

[69] A. Morningstar, L. Colmenarez, V. Khemani, D. J. Luitz, and D. A. Huse, Avalanches and many-body resonances in many-body localized systems, Phys. Rev. B **105**, 174205 (2022).

[70] S. J. Garratt, S. Roy, and J. T. Chalker, Local resonances and parametric level dynamics in the many-body localized phase, Phys. Rev. B **104**, 184203 (2021).

[71] S. J. Garratt and S. Roy, Resonant energy scales and local observables in the many-body localized phase, Phys. Rev. B **106**, 054309 (2022).

[72] D. Wei, A. Rubio-Abadal, B. Ye, F. Machado, J. Kemp, K. Srakaew, S. Hollerith, J. Rui, S. Gopalakrishnan, N. Y. Yao, I. Bloch, and J. Zeiher, Quantum gas microscopy of Kardar-Parisi-Zhang superdiffusion, Science **376**, 716 (2022).

[73] L. S. Levitov and G. B. Lesovik, Charge distribution in quantum shot noise, Pis'ma Zh. Eksp. Teor. Fiz. **58**, 225 (1993) [JETP Lett. **58**, 230 (1993)].

[74] S. Groha, F. H. L. Essler, and P. Calabrese, Full counting statistics in the transverse field Ising chain, SciPost Phys. **4**, 043 (2018).

[75] S. Gopalakrishnan, A. Morningstar, R. Vasseur, and V. Khemani, Distinct universality classes of diffusive transport from full counting statistics, arXiv:2203.09526.

[76] M. Heyl, P. Hauke, and P. Zoller, Quantum localization bounds trotter errors in digital quantum simulation, Sci. Adv. **5**, eaau8342 (2019).

[77] L. M. Sieberer, T. Olsacher, A. Elben, M. Heyl, P. Hauke, F. Haake, and P. Zoller, Digital quantum simulation, trotter errors, and quantum chaos of the kicked top, npj Quantum Inf. **5**, 78 (2019).

[78] C. Kargi, J. P. Dehollain, L. M. Sieberer, F. Henriques, T. Olsacher, P. Hauke, M. Heyl, P. Zoller, and N. K. Langford, Quantum chaos and universal trotterisation behaviours in digital quantum simulations, arXiv:2110.11113.

[79] P. J. D. Crowley and A. Chandran, A constructive theory of the numerically accessible many-body localized to thermal crossover, SciPost Phys. **12**, 201 (2022).

[80] D. M. Long, P. J. D. Crowley, V. Khemani, and A. Chandran, Phenomenology of the prethermal many-body localized regime, Phys. Rev. Lett. **131**, 106301 (2023).

[81] J. yoon Choi, S. Hild, J. Zeiher, P. Schauss, A. Rubio-Abadal, T. Yefsah, V. Khemani, D. A. Huse, I. Bloch, and C. Gross, Exploring the many-body localization transition in two dimensions, Science **352**, 1547 (2016).

[82] J. Šuntajs, J. Bonča, T. Prosen, and L. Vidmar, Quantum chaos challenges many-body localization, Phys. Rev. E **102**, 062144 (2020).

[83] J. Šuntajs, J. Bonča, T. Prosen, and L. Vidmar, Ergodicity breaking transition in finite disordered spin chains, Phys. Rev. B **102**, 064207 (2020).

[84] D. Sels and A. Polkovnikov, Dynamical obstruction to localization in a disordered spin chain, Phys. Rev. E **104**, 054105 (2021).

[85] P. Sierant, D. Delande, and J. Zakrzewski, Thouless time analysis of Anderson and many-body localization transitions, Phys. Rev. Lett. **124**, 186601 (2020).

[86] D. K. Mark, C.-J. Lin, and O. I. Motrunich, Unified structure for exact towers of scar states in the Affleck-Kennedy-Lieb-Tasaki and other models, Phys. Rev. B **101**, 195131 (2020).

[87] S. Moudgalya, N. Regnault, and B. A. Bernevig, η-pairing in Hubbard models: From spectrum generating algebras to quantum many-body scars, Phys. Rev. B **102**, 085140 (2020).

[88] N. O'Dea, F. Burnell, A. Chandran, and V. Khemani, From tunnels to towers: Quantum scars from lie algebras and q-deformed lie algebras, Phys. Rev. Res. **2**, 043305 (2020).

[89] V. Khemani, M. Hermele, and R. Nandkishore, Localization from Hilbert space shattering: From theory to physical realizations, Phys. Rev. B **101**, 174204 (2020).

[90] P. Sala, T. Rakovszky, R. Verresen, M. Knap, and F. Pollmann, Ergodicity breaking arising from Hilbert space fragmentation in dipole-conserving Hamiltonians, Phys. Rev. X **10**, 011047 (2020).